Title	Experimental study on a monovalent inverter-driven water-to-water heat pump with a desuperheater for low energy houses
Author(s)	Blanco, David L.; Nagano, Katsunori; Morimoto, Masahiro
Citation	Applied Thermal Engineering, 50(1), 826-836 https://doi.org/10.1016/j.applthermaleng.2012.07.008
Issue Date	2013-01-10
Doc URL	https://hdl.handle.net/2115/52254
Type	journal article
File Information	ATE50-1_826-836.pdf

Experimental study on a monovalent inverter-driven water-to-water heat pump with a desuperheater for low energy houses

David L. Blanco[1], Katsunori Nagano, Masahiro Morimoto

Division of Human Environmental Systems, Graduate School of Engineering. Hokkaido University, N13-W8. Kita Ku, Sapporo 060-8628, Japan

Abstract

In this study, a novel monovalent inverter-driven water-to-water heat pump with a desuperheater was developed. In this unique system, domestic hot water is produced at a constant temperature controlled by a variable flow rate and stored in a tank. The heat demand is constantly matched by the system through the use of an inverter-driven compressor, which eliminates the need for a buffer tank. Three heating configurations of the system were examined with respect to variable climate conditions and two space heating target temperatures: space heating (mode 1), domestic hot water production (mode 2) and a combination of both (mode 3). Mappings of the performance variables per frequency were constructed for mode 3. For the other modes, the highest COP was identified for each examined climate condition. The difference between modes 1 and 3 was less than 5% for every variable. The space heating target temperature had a strong influence on both modes, showing an average difference of 29% in the COP between 35°C and 45°C. Mode 2 exhibited a considerably reduced COP compared to the other modes, as well as the lowest refrigerant mass flow rate and highest compression ratio among the three modes. From the previous results and the examination of the compressor, the compression ratio presents itself as a key parameter that can help to increase the COP if maintained at low values. The results of this research could be applied to the design of a control methodology for monovalent heat pumps.

Keywords: Ground source heat pump; Heating; Hot water; Coefficient of performance

[1] Corresponding Author
Email: david.blanco.ch@eng.hokudai.ac.jp , david.blanco.ch@gmail.com
Tel /Fax: +81-(0)11-706-6285

NOMENCLATURE

variable name	description and units
Roman characters	
A	area [m^2]
B	circulation pump
DHW	domestic hot water
COP	coefficient of performance
C_p	specific heat at constant pressure [$kJ\ kg^{-1}K^{-1}$]
freq	frequency [Hz]
G	volumetric flow rate [m^3s^{-1}]
H	specific enthalpy [$kJkg^{-1}$]
iHX	internal heat exchanger
$\dot{m}$	refrigerant mass flow rate [kgs^{-1}]
P	pressure [MPa]
P_{ratio}	compressor pressure outlet to pressure inlet ratio
Q	heat transfer [kW]
rpm	revolutions per minute
S	specific entropy [$kJkg^{-1}K^{-1}$]
SH	space heating
step	expansion valve step N.D.
T	temperature [°C]
W_{el}	electrical compressor input [kW]
W_{com}	compression work [kW]
W_{is}	isentropic work [kW]
U	overall heat transfer coefficient [$Wm^{-2}K^{-1}$]
V	volume [m^3]
Greek characters	
κ	polytropic index [N.D.]
η	efficiency [N.D.]
ρ	density [kgm^{-3}]
Subscripts	
c	condenser
crit	critical
cyl	cylinder
d	desuperheater
DHW	domestic hot water
e	evaporator
fr	friction
gas	gas zone
I	primary side
II	secondary side
ind	individual
motor	compressor’s motor
mix	mix zone
lmt	log mean temperature
REFP	NIST REFPROP (Reference Fluid Thermodynamic and Transport Properties)
r	refrigerant
sw	swept
SH	space heating
t	total
uc	uncompressible
v	volumetric
1, 1’, 2, 2’, 3, 3’, 4	junction number

1. Introduction

Because the ecological footprint resulting from the use of non-renewable energy sources continues to grow, heating, ventilation and air conditioning research has focused its attention and efforts on the use of renewable sources. In particular, the constant temperature characteristics of the earth below a depth of ten meters make it ideal for thermal storage and extraction using ground source water-to-water heat pumps (GSHP), especially in harsh environments whose air temperature varies significantly between summer and winter. Through the proper application of heat pump technology, the complete thermal requirements of a low-energy house, including space heating (SH), space cooling, and domestic hot water (DHW), can be fulfilled.

Depending on the local conditions, numerous GSHP configurations are available for providing SH and DHW. In Europe, the most common configuration uses a single-frequency compressor and two alternating hydronic circuits with buffer tanks for each function. However, this system requires a large space for the buffer tanks and to operate the circulation pumps, and it has a low COP when only producing DHW. In the USA, the use of a single-frequency compressor and desuperheater with buffer tanks to provide simultaneous SH and DHW is widespread. In this case, the DHW production is completely determined by the SH or cooling operation, and therefore, the amount of DHW generated is a function of the heat pump runtime [1]. Because of this relationship, auxiliary heaters are necessary to fulfill the DHW load (bivalent system). Such a system uses less space but cannot fulfill the entire demand by itself. Currently, the most common situation in Japan is to use one heat pump for each thermal requirement, which is expensive and requires a large installation area. Recent developments have been concentrated on room type air source R410A heat pumps [2,3] and, since the late 1990s, on CO_2 heat pumps [4], which have been proven to be suitable for DHW generation. More than 5.2 million units of this type of air source CO_2 heat pump have been sold in Japan until 2010 [5]. However, space limitations, government incentives for renewable technology, and an unstable oil market have prompted interest in hybrid solutions that can utilize more than one heat source [6,7] or provide various functions within a single unit [8,9].

In this paper, a new *inverter-driven water-to-water heat pump with a desuperheater* (compact GSHP with a desuperheater) is presented. Unlike the previous systems, this new system applies continuous load control through a variable speed compressor and electronic expansion valve to permanently meet variable heating/cooling demands at the system's highest possible performance. As a result, all of the thermal requirements for a low-energy house can be satisfied using a single unit (monovalent system) throughout the year. As neither the buffer tank for the SH, which is present in other configurations [9], nor the electrical resistances used as a backup during DHW generation [10] are necessary, the system's installation costs and space requirements are lower. In addition, when the system matches the partial load demand using the variable speed compressor, the system works at a higher efficiency, and there is a reduction in electrical consumption and the stress placed on the mechanical components compared to on/off cyclic switching [11].

Despite these advantages, little information is available in the literature about this efficient system, and its market availability is currently nonexistent. This work aims to provide contributions to change this situation. In particular, the objectives of the present work are the following:

1. To characterize the performance of a developed compact GSHP with a desuperheater for three of its operation modes and for two target SH temperatures

under changing climate conditions. The results are useful for designing future systems, and they provide information for evaluating different control strategies to maximize the benefits of the heat pump.

2. To study the behavior of the main compressor parameters and the overall heat transfer coefficients of the heat exchangers. From these results, enhancement opportunities and strategies can be identified for the optimal control of SH, DHW, and the simultaneous operation of both.

2. Operation of the compact GSHP with a desuperheater

The general configuration of the system is illustrated in Fig. 1, in which the numbered junctions in the refrigerant cycle represent a unique refrigerant state between components. On the secondary side of the heat pump, a brine radiant floor heating circuit and fan coil unit are used for the target low-energy house, while DHW is produced in the desuperheater and stored in a tank. The target DHW temperature is achieved by controlling the water flow rate into the desuperheater. The primary side of the heat pump exchanges heat with a brine borehole circuit field, although other configurations of heat exchangers can be explored. The operation modes of the system can be identified using Fig. 1. When DHW is not required and the system is only used for SH (mode 1), the DHW circulation pump, B_{DHW}, is stopped while B_I and B_{II} are active. In this operation mode, heat is extracted from the heat source for use as radiant floor heating during the cold months of the year. When SH is not required, B_I and B_{DHW} are activated while B_{II} is stopped, and the extracted heat is only used for the production of DHW (mode 2). This operation mode is suitable during the transition months between summer and winter. When both SH and DHW are required (mode 3), the three circulation pumps are active, which occurs during winter time. For the hottest days of summer, when cooling is necessary, the internal four-way valves are reversed, and a fan coil unit extracts heat from the conditioned space, which can be used for DHW generation, and injects the remaining heat into the ground.

3. Experimental setup and testing conditions

Fig. 2 illustrates the experimental setup, which is composed of three subsystems: the evaluated compact GSHP with a desuperheater, the test station and the measurement block. Each of these subsystems is described below.

3.1. Experimental setup

3.1.1. Constructed prototype compact GSHP with a desuperheater

A prototype compact GSHP with a desuperheater was developed by our team. Table 1 describes the main characteristics of its components. Indirect contact heat exchangers are commonly used in DHW applications due to safety considerations; therefore, an indirect contact coil type desuperheater was constructed, as shown in Fig. 3. Copper tubes with a smooth surface and flattened region on the upper and lower sides were used for both the refrigerant and water sides to increase the inter-tube contact surface. The resulting heat transfer area was 0.11 m^2. The prototype refrigerant used was R410A, and it was charged to the design conditions of 1.8 kg.

3.1.2. Test station

The prototype was coupled to a test station developed by the authors. This test station can be used to examine any water-to-water heat pump by maintaining user-specified flow rates and temperatures through a PID controlling system on both the primary and secondary sides. The characteristics of the test station components are presented in Table 2. Storage tanks that were filled with a 30% ethylene glycol solution were used to simulate the load and sink of the primary and secondary sides. Auxiliary heat exchangers between the storage tanks enable the reuse of the heat, allowing this system to be close to a standalone device. The temperature of the water flowing into the desuperheater was maintained using a constant temperature circulation bath, while its flow rate was controlled using a variable speed pump.

3.1.3. Measurement system

Table 3 presents the characteristics and related uncertainties in the measurement device. Each sensor was installed at the geometrical center of the connection tubes. The refrigerant mass flow rate was obtained using a Coriolis Effect mass flow meter that was installed in junction 3. A power meter was used to measure the RMS power consumption of the compressor. All of the sensor information was collected and processed in a computer-based data acquisition system.

3.2. Testing conditions

Experiments were conducted according to the northern Japanese climate (Köppen classification Dfb, which is very similar to central European or southeastern Canadian climates) for the heating mode. The flow rates on the primary and secondary sides were fixed at 25 and 16 L min^{-1}, respectively. The target temperature for the production of DHW was set at 65°C in accordance with Japanese consumption patterns and to eliminate legionellae bacteria in the storage tank, which can occur for hot water temperatures between 30 and 45°C [12]. The ground inlet temperature, T_{e1}', was examined at -5, 0 and 5°C, whereas two SH target temperatures, T_{c2}', were considered: 35 and 45°C. The DHW inlet temperature, T_{d2}', was set to 5, 17 and 30°C. The three operational modes described in Chapter 2 were examined. For operational modes 1 and 2, the highest COP for the examined experimental conditions was determined from the variation in the frequency of the compressor. For mode 3, the highest COP for each frequency was evaluated from 45 to 90 Hz in steps of 15 Hz. For each experimental condition described, the expansion valve step was varied until the maximum COP for the specific tested conditions could be identified.

4. Theoretical analysis

The COP is a measurement of the performance of the system, and it is calculated from Eq. (1).

$$COP = \frac{Q_t}{W_{el}} \tag{1}$$

in which

$$Q_t = Q_d + Q_c \tag{2}$$

To increase the COP of the system, Q_t should be increased and/or W_{el} should be decreased. In the following subsections, the heat transfer, specific enthalpy change, and performance of the compressor will be described. Relevant aspects that can contribute to a higher COP will be introduced. The calculations in this section are derived from the following assumptions:

- The insulation of the prototype from its surroundings is perfect.
- The refrigerant is gaseous in the evaporator side of the iHX (junctions 1 and 1' are in the gas zone).
- The refrigerant properties are assumed to be constant between components.
- The pressure drop occurring inside of the expansion valve is isenthalpic.

4.1. Heat balance and refrigeration cycle

The obtained heat transfer rate in the desuperheater, condenser and evaporator was calculated from the non-refrigerant side, as shown in Eq. (3):

$$Q_i = c_{pi} G_i \rho_i \left(T_{i,out} - T_{i,in}\right) \tag{3}$$

where i represents the analyzed heat exchanger and $T_{i,out/in}$ represents the outlet/inlet temperatures of the secondary fluid. By heat balance, heat transfer can also be expressed in terms of the specific enthalpy change of the refrigerant, as shown in Eq. (4):

$$Q_i = \dot{m}\left(H_{i,out} - H_{i,in}\right) \tag{4}$$

From Eq. (4), it is observed that to increase the heat transfer, the specific enthalpy change and/or refrigerant mass flow rate should be increased. Increasing the refrigerant charge in the system, which is possible as long as complete evaporation of the refrigerant is guaranteed before it enters the compressor, could be examined to produce a higher mass flow rate. Using heat exchanger analysis, the LMTD method relates the heat transfer to the overall heat transfer coefficient as follows:

$$Q_i = U_i A_i \Delta T_{i,lmt} \tag{5}$$

Each or all of the factors on the right-hand side of Eq. (5) could be increased to achieve a higher heat transfer rate. However, increasing the heat transfer area is an economical question that will not be addressed. With respect to $\Delta T_{i,lmt}$, a higher compressor discharged temperature would also be beneficial. Regarding U_i, it is of particular interest to examine its behavior against changing environmental conditions.

To plot the refrigeration cycles, the specific enthalpies of junctions 1', 1 and 2 were derived using the refrigerant physical property software REFPROP ver. 8 [13] with the temperature and pressure data of each respective junction for the R410A refrigerant [14]. Heat balance was used to calculate the specific enthalpy of junctions 2' and 3 because they may lie in the mixing zone. Due to the isenthalpic process occurring in the expansion valve, the specific enthalpies of junctions 3 and 4 are the same.

4.2. Compressor efficiencies and swept volume

Because the compressor is a high-efficiency rotary-type inverter-driven compressor, it was desirable to examine how the experimental friction and motor efficiencies behaved under changing conditions and frequencies. The compression work was calculated from Eq. (6):

$$W_{com} = \dot{m}(H_2 - H_1) \tag{6}$$

W_{com} was used to calculate the motor efficiency, η_{motor}, from Eq. (7):

$$\eta_{motor} = \frac{W_{com}}{W_{el}} \tag{7}$$

The isentropic work, W_{is}, was calculated from the entropy of the compressor suction chamber and the outlet pressure using REFPROP:

$$W_{is} = \dot{m}\left(H_{REFP}\left(S_1, P_2\right) - H_1\right) \tag{8}$$

The friction efficiency, η_{fr}, was then determined using Eq. (9):

$$\eta_{fr} = \frac{W_{is}}{W_{com}} \tag{9}$$

Determining the volumetric efficiency is also of considerable importance, and it was determined from Eq. (10):

$$\eta_v = 1 + \frac{V_{uc}}{V_{cyl}} - \frac{V_{uc}}{V_{cyl}} P_{ratio}{}^{\kappa} \tag{10}$$

where P_{ratio} is the ratio between the suction and discharge pressures of the compressor.

To reduce W_{el}, high η_{motor}, η_{fr} and η_v values are desirable. Of particular interest is η_v, which measures how well the refrigerant occupies the available chamber volume in the compressor, as shown in Eq. (11):

$$\dot{m} = \eta_v \rho_1 V_{sw}\, freq \tag{11}$$

Therefore, this parameter is closely related to the mass flow rate and thus the heat transfer rate.

4.3. Overall heat transfer coefficient

The overall heat transfer coefficient in the gas zone was calculated for the indirect contact coil-type desuperheater using geometrical parameters, the Haaland [15] friction factor correlation, the Gnielinski [16] correlation for the Nusselt number and the Schmidt [17] curvature heat transfer enhancement correlation. For the water side, the Haaland [15] and Gnielinski [16] correlations were employed. For the condenser, the correlation presented by Shah [18] was used to model the phase change process. In the evaporator, the Kandlikar [19] correlation was used to model the refrigerant evaporation process by assuming an annular-type flow of refrigerant in the mixing zone. The same correlations used for the gas zone and the water side of the desuperheater were applied for the respective zones of the condenser and evaporator.

4.4. Uncertainty analysis

An uncertainty analysis was conducted based on the theory presented by NIST contained in the program Engineering Equation Solver (EES) [20]. The results are presented in Tables 4 and 5.

5. Results and discussion

In this section, mapping results are presented for the examined conditions and operational modes. The refrigeration cycle of the highest COP for each mode of a particular climate condition is analyzed. Finally, the main parameters of the compressor and the overall heat transfer for each heat exchanger are investigated.

5.1. Performance maps for each operation mode

The maximum heat transferred and COP are shown as a function of T_{e1} for modes 1 and 2 in Fig. 4. The columns represent the heat transferred while the lines represent the COP.

Comparing Q_c obtained for the two target T_{c2}' in Fig.4a, it is observed that the maximum difference between them is only 2.5%. However, it was seen how the COP was drastically reduced 26.0% for the highest T_{c2}'. This interesting result indicates that the COP is primarily affected by a higher electrical consumption when T_{c2}' is raised rather than by a lower heat transfer. Regarding the frequency of the compressor, the highest COP for each T_{e1} was found at 45 Hz, which is close to the fundamental frequency (50 Hz). At these frequencies, the compressor reduces its inverter losses, and its electrical efficiency increases.

The impact of T_{d2}' on the Q_d and COP in mode 2 can be observed in Fig. 4b. Note that the lowest T_{d2}' for this mode was 8°C due to the high DHW flow rates. The greatest variation of Q_d between the examined T_{d2}' was close to 10.3%, whereas the COP exhibited a greater variation of 18.1%. Again, the variation in COP is explained by the increased electrical consumption between the two target T_{c2}'. Moreover, the highest heat transfer and COP were observed for the lowest T_{d2}'. Consequently, to have a high COP for the current mode, water directly from the tap or from the bottom of the DHW tank should be used as inlet to the desuperheater. Additionally, it was observed that when T_{e1} = -5°C, T_2 cannot reach the target T_{d2} for low frequencies, despite the evaluated T_{d2}'. In this extreme condition, the highest COP was obtained only at 90 Hz, whereas it was observed at 45 Hz for ground temperatures of 0 and 5°C. This result explains the higher Q_d when T_{e1} = -5 compared to T_{e1} = 0 and 5°C.

For mode 3, performance figures were produced and compared to mode 1 and are shown in Fig. 5 for the three examined T_{d2}' values. For each T_{c2}', the electrical consumption W_{el} (bottom), total heat transfer Q_t (middle), and COP (top) are related to the compressor frequency. It is evident from the bottom of the figure that T_{e1} has a minimal impact on W_{el}. However, it was observed that this impact increases slightly with the compressor frequency.

For T_{c2}' = 35°C, the greatest difference in W_{el} between the highest and lowest T_{e1} values was 7.3%, whereas it was 7.4% when T_{c2}' = 45°C. However, the average increase in W_{el} when T_{c2}' was increased was 18.0%, which indicates the great sensibility of this factor. When focusing on Q_t, a considerable difference with regard to T_{e1} is observed. Again, this difference is directly proportional to the frequency. For T_{c2}' = 35°C, the greatest difference in Q_t between the highest and lowest T_{e1} values was 40.0%, whereas it was 29.5% for T_{c2}' = 45°C. Examining the change with respect to T_{c2}', Q_t was found to be reduced by an average of 8.3% when T_{c2}' was increased.

The combination of the previous effects clearly impacts the COP, as shown in the top of the figure. An important decrease of 29.0% in average between the two examined T_{c2}' was observed. From these results, it is clear that maintaining a low SH target temperature is desirable to maintain a high COP; therefore, radiant floor heating should be chosen over fan-and-coil type heaters when possible. Finally, note that modes 1 and 3 do not differ significantly in terms of W_{el} or the total heat transferred, and the difference in COP is less than 5%.

It is also interesting to examine the relationship between the two heating functions (SH and DHW) in mode 3. Fig. 6 presents the heat transferred for Q_c and Q_d and its relation to Q_t. The linearity of the results despite the different values of T_{d2}' is remarkable. This behavior suggests that for fixed operating conditions, the thermodynamic process of condensation changes very little with respect to the presence of DHW, which will be further clarified in subsection 5.3, which discusses the refrigeration cycles of each mode. For T_{c2}' = 35°C, the proportion of Q_d to Q_t remained within 11.0% and 32.0%, with an average of 20.0%. For T_{c2}' = 45°C the proportion increased to between 35.0% and 67%, with an average of 44.0%. Thus, the condensation process is strongly related to T_{c2}'. In fact, if T_{c2}' is increased to a value close to T_{d2}, the entirety of Q_t would be used for DHW, which would result in equivalence with mode 2. This result is extremely important because improper management of T_{c2}' might result in a system that is incapable of fulfilling either the DHW or SH demand, thereby violating the working principle of the machine.

5.2. Comparison of operation modes according to the compressor's frequency

It is useful to compare the performance of the system for the three operation modes at changing compressor frequencies. This comparison is shown in Fig. 7 for the three examined T_{e1} temperatures. For modes 1 and 2, the compressor was tested at 45 and 60 Hz, as described in subsection 3.2, whereas all of the frequencies were considered for mode 3. For the three cases, the W_{el} of modes 1 and 3 exhibits practically the same behavior irrespective of the operation frequency, contrary to mode 2, in which W_{el} is clearly larger for every examined condition. The same situation is observed for Q_t as for W_{el}. Modes 1 and 3 exhibit differences of less than 3.2%, and the change in Q_t with respect to frequency is the same for both modes. However, for mode 2, Q_t was much lower than those in the other modes for every examined frequency. These differences have an impact on T_2 and the COP of the system, as observed in the top of the figure. As expected, mode 3 requires that T_2 be above the target T_{d2}, whereas this condition does not apply for mode 1, which results in a slight difference between the two temperatures. However, mode 2 exhibits a temperature that is considerably greater than those in the other two modes for every T_{e1}. Consequently, the COPs of modes 1 and 3 are similar, whereas that of mode 2 is considerably lower. The COP and other performance variables related to each condition and mode are presented in Table 6. The highest COP of the system was observed to be 4.75, 2.20 and 4.50 for modes 1, 2 and 3, respectively. To understand these enormous differences in performance, the refrigeration cycles must be examined.

5.3. Comparison of PH diagrams for each operational mode

At this point, a comparison of the three operational modes in the PH diagrams at the same experimental conditions is necessary, as shown in Fig. 8 for both SH target temperatures. Similarities in the condensation process of modes 1 and 3 were observed for the two T_{c2}' values. Specifically, the condensation pressure does not change despite the production of DHW because of the large difference between G_d and G_c, which impacts the heat transfer for each application. Furthermore, this behavior accounts for the small difference between the variables with respect to T_{d2}' in Fig. 5. Because G_d is directly related to the target T_{d2} and the size of the desuperheater, these variables should be carefully controlled to avoid a decrease in the COP of the system.

For T_{c2}' = 35°C, the state of the refrigerant at junction 1 was almost identical for the three operational modes. The compression process was also very similar. Despite this result, the mass flow rate of mode 2 decreased by 19.9% compared to mode 3. This reduction can be explained as follows. Although the compression ratios of modes 1 and 3 were almost identical, the higher compression ratio required for mode 2 was achieved by closing the expansion valve further. This extremely high compression ratio decreased the volumetric efficiency of the compressor. A smaller expansion valve opening and lower volumetric efficiency combine to produce a reduction in the refrigerant mass flow rate. As a result, the heat transfer and specific enthalpy change were substantially affected. However, when T_{c2}' = 45°C, a higher compression ratio was also required for modes 1 and 3, and the specific enthalpy change in the heat exchangers decreased. As the system should maintain the discharged refrigerant temperature of the compressor above the target DHW temperature while also providing a high pressure outlet to produce the target SH outlet temperature, the expansion valve had to be closed even further for mode 3. This behavior explains the variation in the refrigerant mass flow rates between modes 1 and 3.

The previous analyses are summarized in the column graphs of COP and Q_t, which are shown on top of the PH diagrams. The black column represents the heat transferred for DHW in mode 3, which is directly proportional to T_{c2}', as discussed previously. The highest COP is achieved for mode 1, followed closely by mode 3. As expected, the COP of mode 2 is only 48.9% of that achieved for mode 3 at $T_{c2}' = 35°C$. Now that the difference in the operation modes is clear, it is necessary to seek strategies for coping with these performance differences for correct operation of the system.

5.4. Compressor performance

To understand how the compressor affects the COP of the system for the two SH target temperatures, its main parameters were analyzed. The motor, friction and volumetric efficiencies and the pressure ratio related to the COP of the system are shown in Fig. 9.

The motor efficiency (η_{motor}) was observed to be greater than 0.80 for all but one experiment, whereas the friction efficiency (η_{fr}) averaged 0.87 and had variance close to 0.05. However, a direct relationship with the COP of the system could not be extracted. In contrast, the P_{ratio} and η_v were observed to be strongly correlated to the COP. In general, the experiments for the highest T_{c2}' have a higher P_{ratio} and exhibit a lower COP. This high P_{ratio} negatively affects η_v, which in turn reduces the refrigerant mass flow rate. As a consequence, a directive can be stated that to maintain a high COP, the P_{ratio} should be kept as low as possible in the system. In fact, the highest observed COP was for the lowest P_{ratio} and highest η_v. By applying this directive, a reduction in W_{el} and an increase in the mass flow rate could be achieved.

5.5. Overall heat transfer coefficient analysis in the heat exchangers

The behavior of the overall heat transfer coefficients of the desuperheater (U_d), condenser (U_c) and evaporator (U_e) against changing conditions is shown in Fig. 10. The left column of this figure shows the relation of each coefficient with the COP of the system, whereas the right column displays the relation with respect to the refrigerant mass flow rate. Because DHW is produced at a variable flow rate, Fig. 10a shows U_d categorized by G_d. It is observed that U_d is not directly related to G_d or the COP of the system. Actually, the highest observed COP is not observed for the highest U_d because the COP is a global measurement of the system that indirectly considers the performance of each individual component and their relationship. However, U_d is clearly shown to be directly related to the refrigerant mass flow rate, as is evident from the right side of the figure. This observation is explained by the fact that U_d is dominated by the lowest fluid convective heat transfer coefficient, which corresponds to the refrigerant in this case.

A similar situation holds for the condenser and evaporator, as shown in Figs. 10b and c, where no clear relationship with respect to the COP can be established. Nevertheless, on the graphs in the right side of the figure, it is observed that U_c and U_e increased according to the refrigerant mass flow rate, especially in the gas zone. However, only a very small difference was observed when the refrigerant changes its phase, even with respect to the two examined T_{c2}' values. These results suggest that the heat transfer is slightly dependent on the condensation or evaporation pressures but strongly dependent on the refrigerant mass flow rate. Independent studies report the same tendency at low reduced pressures (P_2/P_{crit}) [21] and near-critical pressures [22]. The pressures obtained in the present study confirm this tendency at moderate reduced pressures. A second directive can be extracted from the previous analysis: to maintain a high COP, the refrigerant mass flow rate should be maintained as high as possible to enable a higher heat transfer. This directive is directed towards increasing Q_t.

The results of these analyses can be applied to incorporate mechanisms directed towards reducing the gap in COP between mode 2 and the other modes. Furthermore, a control strategy can be established that directs proper management of the heating loads.

6. Conclusions

1. A novel prototype monovalent inverter-driven water-to-water heat pump was developed, and its performance was analyzed with respect to varying climate and control conditions. Performance figures were constructed that present the highest COP, total heat transfer, and electrical consumption of the system based on the frequency of the compressor and the DHW inlet temperature. Three operation modes were examined. For every evaluated climate condition, the difference in the COP between space heating only (mode 1) and combined space heating and domestic hot water production (mode 3) was less than 5%. However, domestic hot water production (mode 2) exhibited a much lower performance. For a target space heating temperature of 35°C and a ground inlet temperature of 5°C, the highest COP was 4.75 for mode 1 and 4.50 for mode 3. For mode 2, the highest COP was 2.20.
2. In mode 3, the proportion of domestic hot water to the total heat transfer remained rather constant irrespective of the compressor frequency, and it is strongly related to the target space heating temperature. For the lowest target space heating temperature, the average domestic hot water heat transfer was 20%. At 45°C, this transfer increased to 44%.

3. The analyses of the PH diagrams for each mode revealed similar compression processes, condensation pressures, and enthalpy changes for modes 1 and 3. However, the compression ratio drastically increased for mode 2, and its mass flow rate decreased by 19.9%.
4. A low compression ratio was identified as an important parameter of the compressor that can contribute to maintaining a high volumetric efficiency and thus low electrical consumption. In fact, the highest COP for mode 3 was observed in the experiment with the lowest compression ratio.
5. The study of the desuperheater revealed that the overall heat transfer coefficient was almost invariable to varying water flow rates, which indicates the need to increase the refrigerant side convective heat transfer coefficient. Practically no influence of the two examined space heating target temperatures on either the condensation or evaporation heat transfer coefficients was observed. A high refrigerant mass flow rate was identified as an important characteristic for all heat exchangers that can contribute to maintaining a high heat transfer in each heat exchanger.
6. The results of this research are useful for designing future monovalent heat pumps and can be applied in the development of control strategies aimed at fulfilling the thermal requirements of a low-energy home.

7. Acknowledgements

The authors would like to thank Sunpot Co. Ltd. for the development of the prototype and continuous support during the project. In addition, we would like to thank Mr. Nakamura from Hokkaido University as well as Mr. Umezawa and Ph.D. Katsura for their fruitful discussions. The financial support from the Ministry of Education, Culture, Sports, Science and Technology of Japan is deeply appreciated.

8. References

[1] D.B. Loyd, The smart guide to Geothermal: How to harvest Earth's free energy for heating & Cooling, PixyJack Press 1st Ed, 2011.

[2] M. Gommori, S. Yoshinaga, Development of high efficiency and instantaneous heat-pump water heating system using R410A, Reito Journal (JSRAE) 79 No. 917 (2004) 203-208.

[3] S. Okoshi, K. Irisawa, R410A heat pump hot water supply system for commercial use, Reito Journal (JSRAE) 79 No. 917 (2004) 209-213.

[4] P. Nekså, H. Rekstad, G. Zakeri, P. Schiefloe, CO_2-heat pump water heater: characteristics, system design and experimental results. Int. J. Refrigeration 21 No. 3 (1998) 172-179.

[5] IEA HPP Annex 32, Economical heating and cooling systems for low energy houses, IEA HPP Report No.HPP-AN32-1 (2011).

[6] O. Ozgener, A. Hepbasli, Performance analysis of a solar assisted ground-source heat pump system for greenhouse heating: An experimental study. Build Environ. 40 (2005), 1040–1050.

[7] H. Wang, C. Qi, E. Wang, J. Zhao, A case study of underground thermal storage in a solar-ground coupled heat pump system for residential buildings. Renew Energ. 34 (2009), 307-314.

[8] S. K. Chou, K. J. Chua, J. C. Ho, C. L. Ooi, On the study of an energy-efficient greenhouse for heating, cooling and dehumidification applications. Appl. Energ. 77 (2004), 355-373.

[9] J. Stene, Residential CO_2 heat pump system for combined space heating and hot water heating, Int. J. Refrigeration 28 (2005) 1259-1265.

[10] A. L. Biaou, M. A. Bernier, Achieving total domestic hot water production with renewable energy, Build. Environ. 43 (2008) 651-660.

[11] C. Aprea, R. Mastrullo, C. Renno, Determination of the compressor optimal working conditions, Appl. Therm. Eng. 29 (2009) 1991-1997.

[12] M. Alary, J. Joly, Risk factor for contamination of domestic hot water systems by legionellae, Appl. Environ. Microbiol., 57 No. 8 (1991) 2360-2367.

[13] E.W. Lemmon, M.L. Huber, M.O. McLinden, NIST Standard Reference Database 23: Reference Fluid Thermodynamic and Transport Properties-REFPROP, Version 8.0, National Institute of Standards and Technology, Standard Reference Data Program, Gaithersburg, 2007.

[14] E.W. Lemmon, Pseudo Pure-Fluid Equations of State for the Refrigerant Blends R-410A, R-404A, R-507A, and R-407C, Int. J. Thermophys., 24 (2003) 991-1006.

[15] S. E. Haaland, Simple and explicit formulas for the friction factor in turbulent pipe flow, J. Fluids Eng. 105 (1983) 89-90.

[16] V. Gnielinski, New equations for heat and mass transfer in turbulent pipe and channel flow, Int. Chem. Eng. 16 (1976) 359-368.

[17] E. Schmidt, Wärmeübergang und druckverlust in rohrschlangen, Chem. Ing. Tech. 39 No.13 (1967) 781-789.

[18] M. M. Shah, A general correlation for heat transfer during film condensation in pipes, Int. J. Heat Mass Tran. 22 (1979) 547-556

[19] S. Kandlikar, A general correlation for saturated two-phase flow boiling heat transfer inside horizontal and vertical tubes, J. Heat Transfer 112 (1990) 219-228.

[20] B.N. Taylor, C.E. Kuyatt, Guidelines for Evaluating and Expressing the Uncertainty of NIST Measurement Results, National Institute of Standards and Technology Technical Note 1297, 1994.

[21] W.S. Kuo, Y.M. Lie, Y.Y. Hsieh, T.F. Lin, Condensation heat transfer and pressure drop of refrigerant R-410A flow in a vertical plate heat exchanger, Int. J. Heat Mass Tran. 48 (2005) 5205-5220.

[22] S. Garimella, Near critical/supercritical heat transfer measurements of R-410A in small diameter tube. Georgia, USA. Georgia Institute of Technology, prepared for Air-Conditioning and Refrigeration Technology Institute (2008) ARTI Report No. 20120-01.

List of Figures

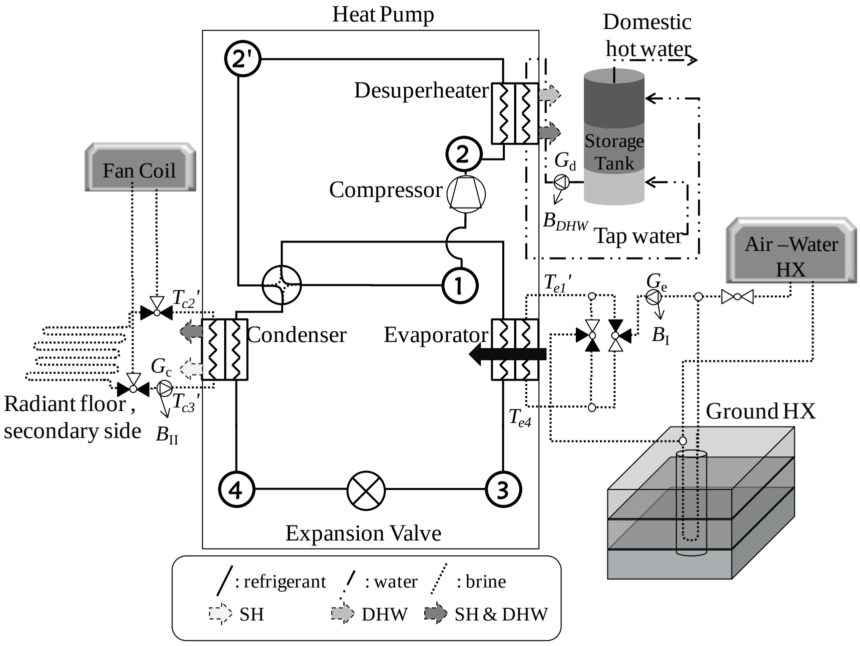

a) Operation scheme

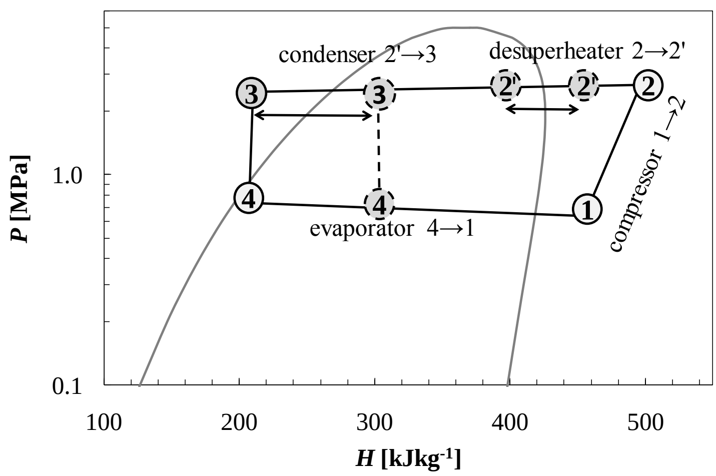

b) Representation of the SH and DHW modes in the PH diagram (Refrigerant: R410A)

Fig. 1. Compact GSHP with a desuperheater

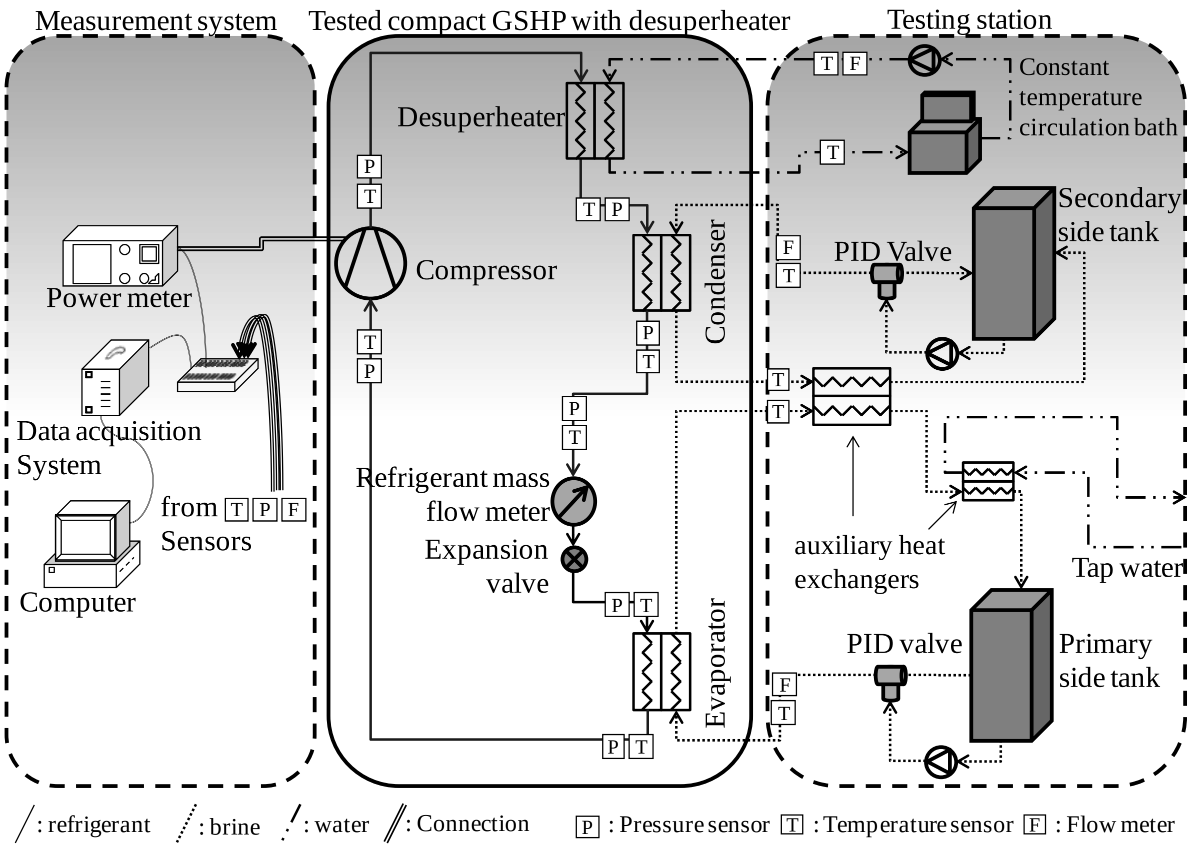

Fig. 2. Experimental setup for testing the prototype compact GSHP with a desuperheater

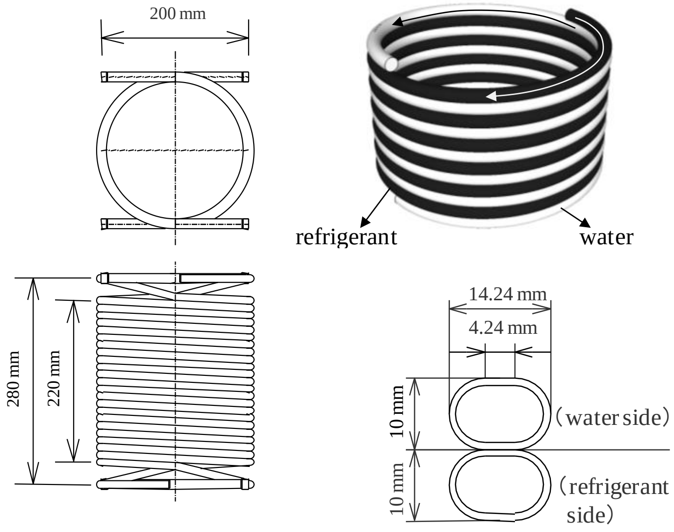

Fig. 3. Construction of the indirect contact coil-type desuperheater

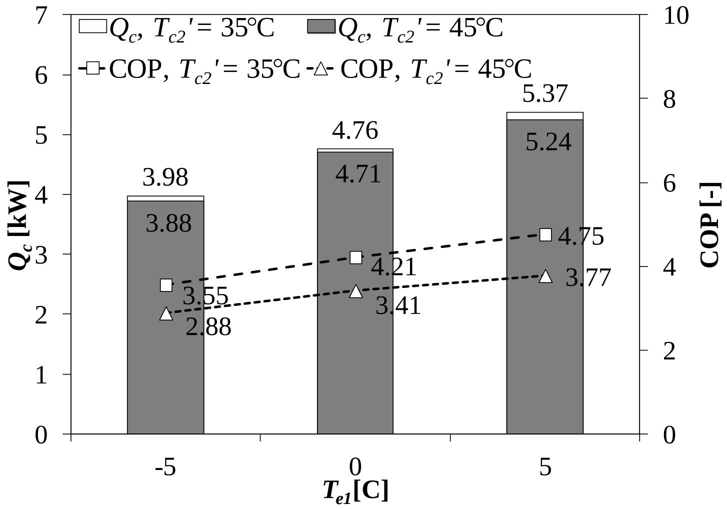

a) SH (mode 1)

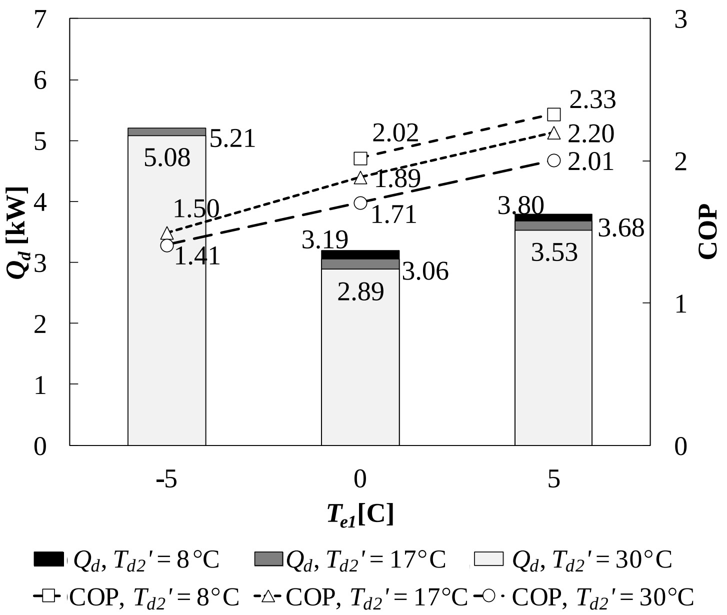

b) DHW (mode 2)

Fig. 4. COP and Q_t for modes 1 and 2 related to T_{e1} for the three examined domestic hot water inlet temperatures

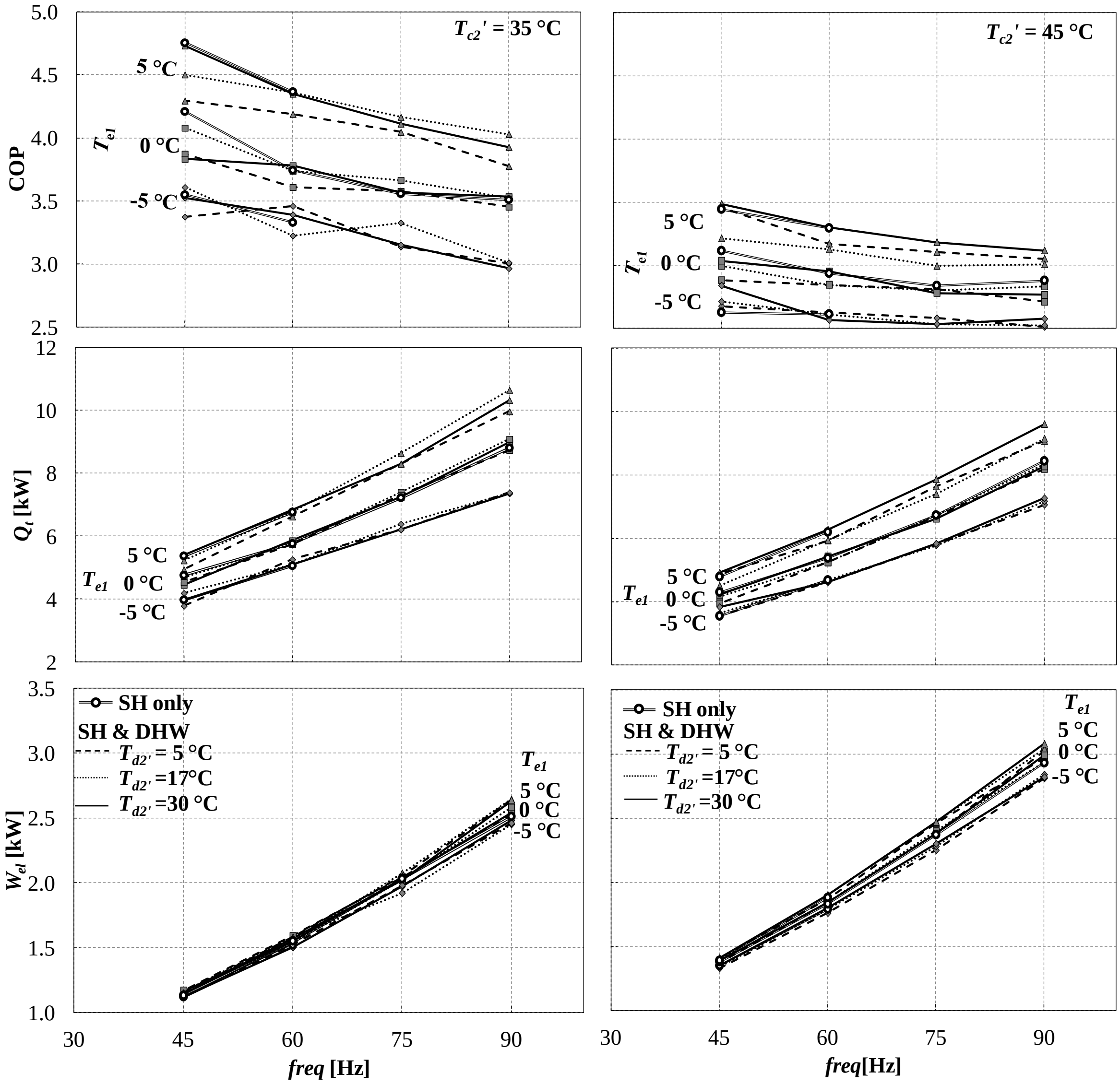

a) $T_{c2}' = 35$ °C b) $T_{c2}' = 45$ °C

Fig. 5. COP, Q_t and W_{el} related to the compressor frequency for the three examined domestic hot water inlet temperatures

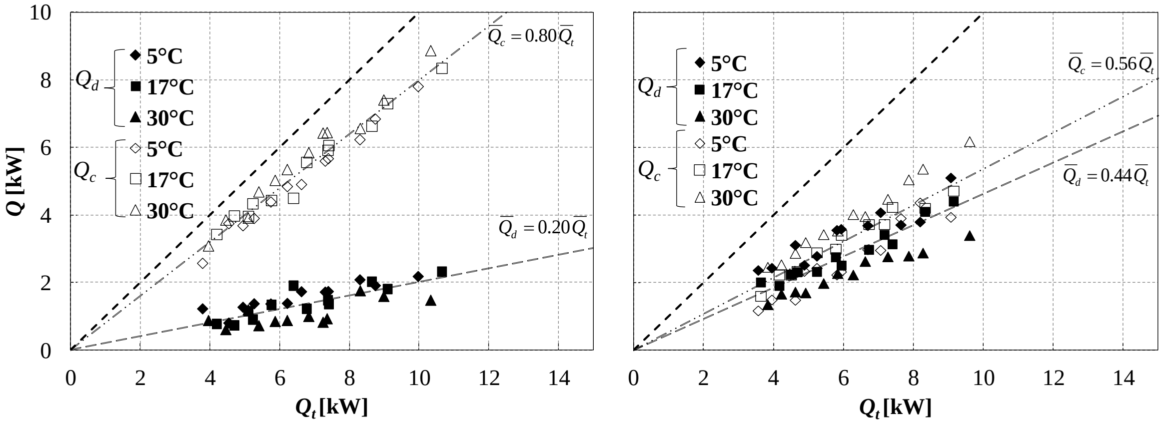

a) T_{c2}' = 35 °C b) T_{c2}' = 45 °C

Fig. 6. Heat transfer for SH and DHW related to Q_t for the three examined domestic hot water inlet temperatures in mode 3.

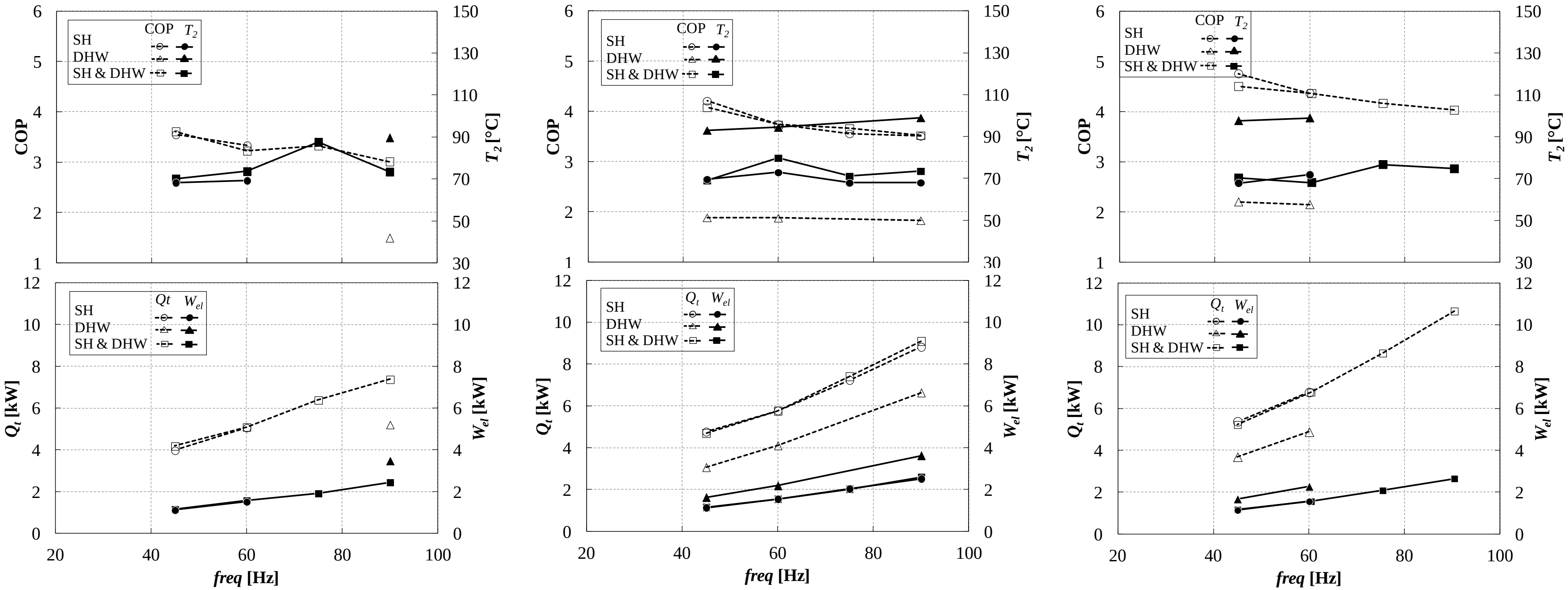

a) T_{e1} = -5 °C b) T_{e1} = 0 °C c) T_{e1} = 5 °C

Fig. 7. Comparison of the outlet temperature of the compressor, COP, Q_t, and W_{el} of the compact GSHP with a desuperheater, related to the compressor frequency, for the three operational modes (T_{d2}' = 17°C, T_{c2}' = 35°C)

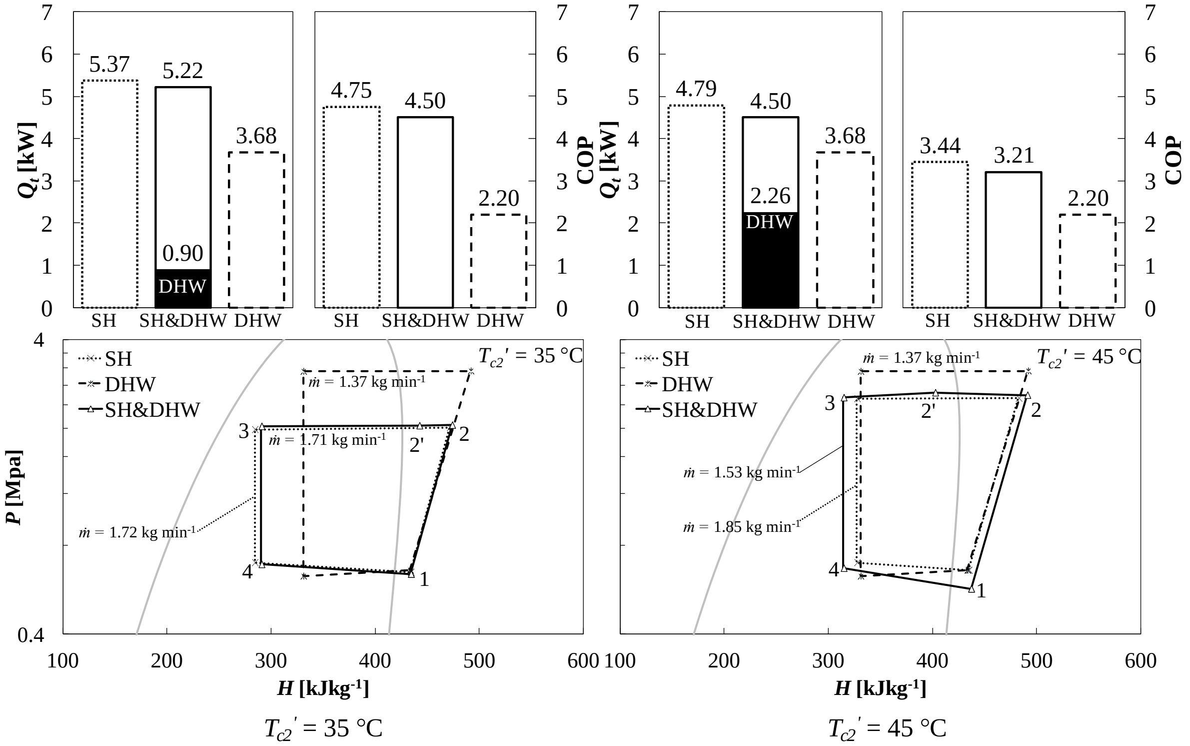

Fig. 8. COP, total heat transfer, and refrigeration cycle in the PH diagram for the three operational modes (*freq* = 45 Hz, T_{e1} = 5°C, T_{d2}' = 17°C, T_{c2}' = 35°C and 45°C)

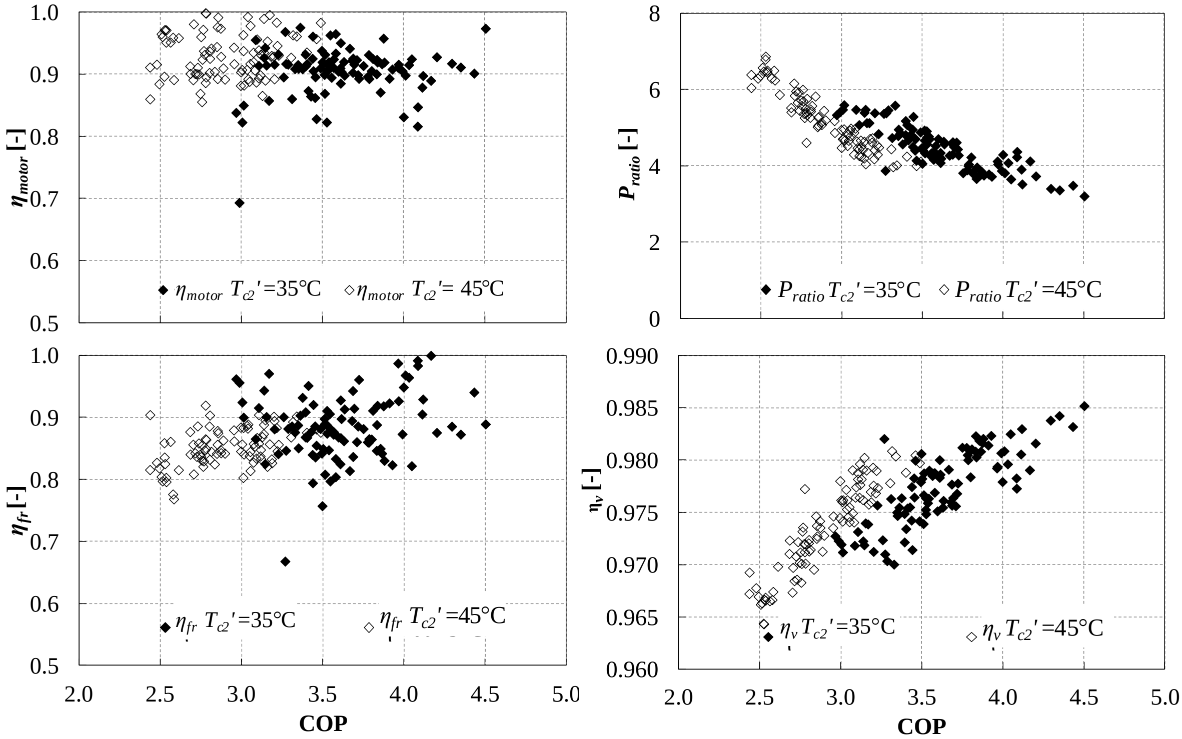

Fig. 9. Efficiencies of the compressor (η_{fr}, η_{motor}, η_v) and compression ratio (P_{ratio}) related to the COP of the system

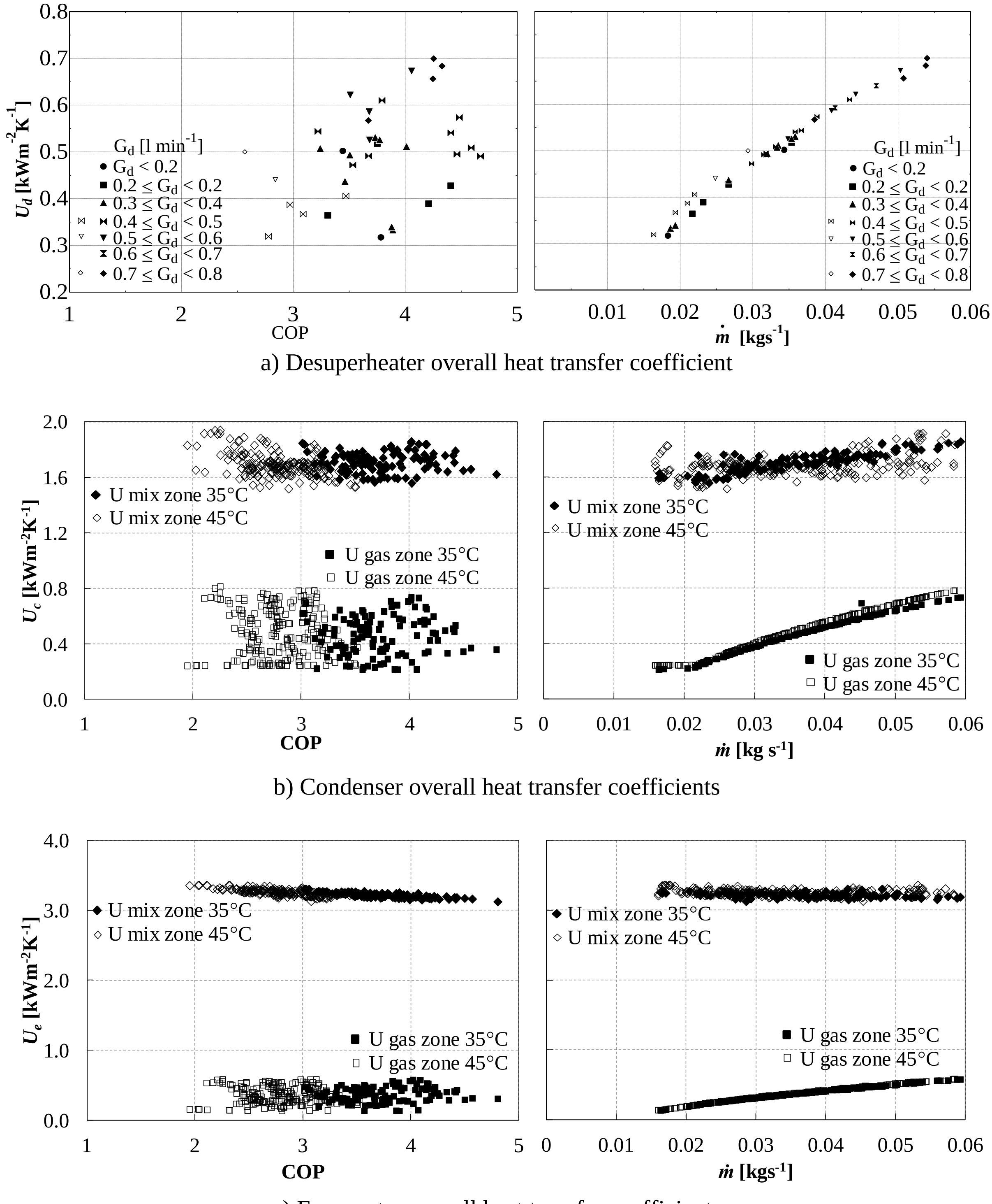

a) Desuperheater overall heat transfer coefficient

b) Condenser overall heat transfer coefficients

c) Evaporator overall heat transfer coefficients

Fig. 10. Overall heat transfer coefficients for the respective refrigerant zones in each heat exchanger and their relation with the COP (left) and refrigerant mass flow rate (right). Black/white markers refer to T_{c2}' = 35/45 °C

List of Tables

Table 1. Main components of the prototype compact GSHP with a desuperheater

Component	**Type**	**Properties**
Compressor	R410A refrigerant, rotary type, Inverter drive	W_{el} < 2 kW, 900-7,200 RPM, T < 200°C
Condenser and Evaporator	Brazed plate heat exchanger	P < 4.5 MPa, 528 × 112 × 82*, A_c, A_e = 1.4 m^2
Desuperheater	Indirect contact, coil	Smooth surface, copper to copper tube contact, A_d = 0.11 m^2
Expansion valve	Electronic, bi-flow	0 to 4.2 MPa, full opening: 5.5 mm, Step controlled, 10-480

* height × width × depth [mm]

Table 2. Description of test station components

Component	Type	Properties
Circulation pump	Electrical	50 Hz, 3.7 kW
Pump inverter	Three-phase induction motor	3 kW, 0.2 < *freq* < 400 Hz,
Flow valve	PID-controlled valve	P < 1 MPa, ± 2%
Indicator	Digital temperature indicator	-200 to 1,370°C, ± 0.1%, sampling period: 250 ms
Flow meter	Magnetic flow meter	-40 < T < 160°C, ± 0.1%
Aux HX main	Gasket plate type	D = 780 × 340 × 350*, A = 2.5 m^2
Aux HX secondary	Gasket plate type	D = 480 × 180 × 150*, A = 0.34 m^2
DHW circulator	Constant temperature chamber	-47 to 150°C, 850 W cooling at 20°C ± 0.5%

* height × width × depth [mm]

Table 3. Description of the measurement system components

Component	Type	Properties
Pressure sensors	Semiconductor pressure sensor	In-tube installation, P < 50 MPa, ± 0.01%
Temperature sensors	PT100	In-tube installation, -30 < T < 200°C ± 0.03%
Mass flow meter	Coriolis effect	G_r < 100 L/h, -40<T<125°C, ± 0.5%
Data acquisition with computer	Digital measuring station	Sample rate = 250 ms, ± 0.05%
Power meter	Electronic power meter	RMS voltage/current measurement, ± 0.1%

Table 4. Performance uncertainty analysis for the three operation modes

Operation Mode	**COP**	$\boldsymbol{Q_c}$ **[kW]**	$\boldsymbol{Q_d}$ **[kW]**	$\boldsymbol{Q_e}$ **[kW]**
SH	$\pm 2.24\times10^{-2}$	$\pm 2.04\times10^{-2}$	-	$\pm 6.9\times10^{-3}$
DHW	$\pm 3.8\times10^{-3}$	-	$\pm 8.7\times10^{-3}$	$\pm 5.8\times10^{-3}$
SH & DHW	$\pm 2.23\times10^{-2}$	$\pm 2.03\times10^{-2}$	$\pm 5.4\times10^{-3}$	$\pm 8.8\times10^{-3}$

Table 5. Uncertainty analysis of the compressor

T_{c2}'	η_{motor}	η_{fr}	η_v	P_{ratio}
35°C	$\pm 5.86\times10^{-4}$	$\pm 5.16\times10^{-3}$	$\pm 1.72\times10^{-7}$	$\pm 7.91\times10^{-4}$
45°C	$\pm 5.70\times10^{-4}$	$\pm 5.28\times10^{-3}$	$\pm 1.90\times10^{-7}$	$\pm 9.71\times10^{-4}$

Table 6. Summary of the highest COP at the same climate conditions for all of the evaluated configurations (T_{c2}' = 35°C, T_{d2}' = 17°C, T_{d2} = 65°C)

T_{e1} [°C]	mode	*freq* [Hz]	Q_d [kW]	Q_c [kW]	W_{el} [kW]	P_{ratio}	COP
-5	SH	45	-	3.98	1.12	4.32	3.55
	DHW	90	5.21	-	3.48	6.33	1.50
	SH & DHW	45	0.77	3.42	1.16	4.34	3.61
0	SH	45	-	4.76	1.13	3.49	4.21
	DHW	45	3.06	-	1.62	5.13	1.89
	SH & DHW	45	0.73	3.96	1.15	4.04	4.08
5	SH	45	-	5.37	1.13	3.09	4.75
	DHW	45	3.68	-	1.67	4.74	2.20
	SH & DHW	45	0.90	4.32	1.16	3.20	4.50